COBEM 2021 26th International Congress of Mechanical Engineering
November 22-26, 2021, Virtual Congress, Brazil

COB-2021-1808
SYSTEM IDENTIFICATION AND CONTROLLER DESIGN FOR THE HIGH-DYNAMIC DOUBLE-CRYSTAL MONOCHROMATOR AT SIRIUS

Ricardo Malagodi Caliari
Niederauer Mastelari
State University of Campinas (UNICAMP)
ricardo.caliari@gmail.com, niede@fem.unicamp.br

Marcelo Alexandre Leite de Moraes
Brazilian Center for Research in Energy and Materials (CNPEM)
marcelo.moraes@lnls.br

Renan Ramalho Geraldes
Brazilian Center for Research in Energy and Materials (CNPEM)
Eindhoven University of Technology (TU/e)
renan.geraldes@lnls.br

Gert Witvoet
Eindhoven University of Technology (TU/e)
g.witvoet@tue.nl

Abstract. *A 4th generation of storage ring light sources is emerging to push the X-rays brightness and coherence fraction to unprecedented levels. As a consequence, a breakthrough is expected in science opportunities in terms of temporal and spacial resolutions. Yet, in order to allow the experiments to profit from the progress of the storage rings, their experimental stations, the so-called beamlines, must evolve and perform accordingly. Then, after decades of well-established solutions, several beamline instruments may now need to go through a paradigm shift. With the construction of the new Sirius Storage Ring, since 2015 the Brazilian Synchrotron Light Laboratory (LNLS) has developed the High-Dynamic Double-Crystal Monochromator (HD-DCM) for X-rays. Indeed, understanding that the traditional approach of high-stiffness design and mitigation of disturbances would be close practical limitations in existing X-ray monochromators, the HD-DCM is the first to implement a low-stiffness mechanical design concept with high closed-loop mechatronics performance. Its development was based on predictive design to realize it "first time right" and deliver positioning performance improvements by factors of 4 and 100 with respect to state-of-the-art DCMs, in fixed-energy and scanning modes, respectively. The main project target number was 10 nrad RMS in pitch control error integrated up to 2.5 kHz which could only be achieved by means of a closed loop control projected with the bandwidth in the range of 200 to 250Hz. The real time system operates in an update rate of 20kHz, what makes it possible in use many well-known continuous controller design techniques. In this work, the loop-shaping technique is implemented to achieve the desired bandwidth with the phase and gain margin robustness targets. Moreover, methods and results of detailed plant identifications that were essential to ensure a robust design and to guarantee a safe operation at different conditions are also discussed here. Then, the final controller design is presented with bode plots, open-loop, sensitivity and Nyquist diagrams. The fixed-energy control errors are the most straightforward numbers to be compared with the pitch angular error in existing DCMs in synchrotron beamlines. Yet, in the case of this system, the scanning modes are discussed in a deeper level, because we proved to keep the small pitch angular errors even at high energy scanning velocities, which is an unprecedented achievement for this kind of machine. These characteristics shall be beneficial for the Sirius scientists to in terms of experimental accuracy and throughput, also possibly opening new scientific opportunities.*

Keywords: *loop-shaping, control design, mechatronics, high-precision, synchrotron*

1. INTRODUCTION

This work presents the system identification, the closed-loop controller design by loop-shaping and control performance results of the High-Dynamic Double-Crystal Monochromator (HD-DCM) [1], which has been developed since 2015 for X-rays beamlines of Sirius 4th-generation light source at the Brazilian Synchrotron Light Laboratory (LNLS) [2]. Being the first DCM to implement a low-stiffness mechanical design concept with high closed-loop mechatronic performance, its development was based on predictive design to realize it "first time right" and deliver positioning performance improvements by factors of 4 and 100 with respect to state-of-the-art DCMs, in fixed-energy

and scanning modes, respectively. The system identification techniques presented here focus on the high-performance module of the machine, a 3-degree-of-freedom (DoF) sub-nanometer resolution positioning stage, using well-known multiple-input and multiple-output (MIMO) identification approaches. Thanks to a careful mechanical design aiming at the final mechatronic concept, the MIMO system is sufficiently decoupled to be addressed as independent single-input and single-output (SISO) systems, such that the controllers can be designed for each individual DoF separately, according to well-established control design targets and criteria, by means of loop-shaping through frequency domain analysis [3].

2. MECHANICAL DESIGN

A DCM at a synchrotron beamline is an optical component that selects the desired photon energy/wavelength for a given experimental analysis related to materials characterization. In this case, the desired outgoing wavelength is selected according to Bragg's law of diffraction, by controlling the incidence angle of a broad-band incident beam with respect to the surface of two subsequent silicon monocrystals, which must remain parallel to each other, but with variable gap to keep a fixed-exit beam . Operational ranges and more details about this implementation can be found in [4].

Figure 1 shows the downstream view of the core of the HD-DCM and depicts the complete mechanical schematics with its main elements, including two sets of silicon crystals, which can be alternatively selected by the users for different energy ranges and resolutions. Because of complex cryocooling solutions to handle high power loads, the first crystals (8) were chosen to be rigidly fixed to its metrology frame (7) and, finally, to the main rotating frame (5) via the auxiliary mounting frame (6). Then, all the relative DoF that are necessary for fine positioning between crystals are limited to the second crystals (12), which can be cryocooled with more compliant copper braids, and their metrology frame (11). Therefore, aiming at the highest repeatability and mechanical stability performance, only the essential positioning DoFs were implemented in the so-called crystal cage (as opposed to different DCM designs with redundant or complementary positioning stages), namely: the translation for the gap between the crystals; and two rotations, pitch and roll, for parallelism tuning.

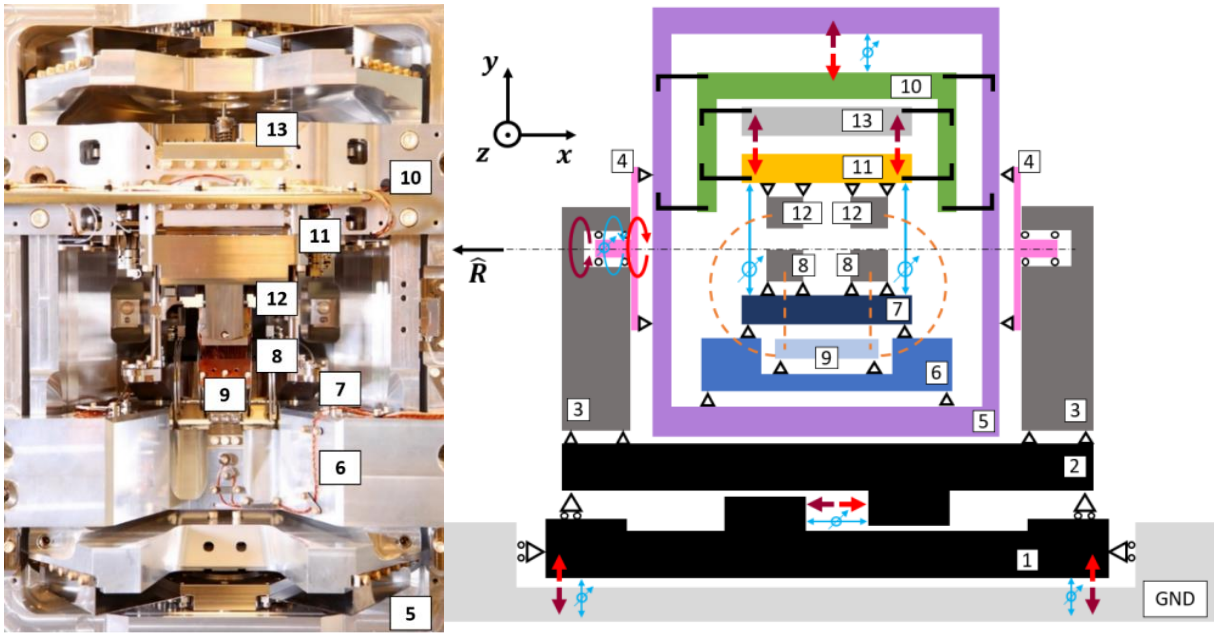

Figure 1 - Core of the HD-DCM (left) and HD-DCM schematics (right): GND; bottom granite block (1); top granite block (2); towers (3) with the stators of the two rotary bearings; rotors of the two bearings (4); main rotating frame (5); auxiliary mounting frame (6); metrology frame of 1st crystals (7); 1st crystals (8); cooling manifold (9); long-stroke frame (10); metrology frame of the 2nd crystals (11); 2nd crystals (12); and balance mass (13).

Since a mechanism with several millimeters of range and nanometer-level performance as a single motion stage may find severe practical concretization limitations, a concept using long-stroke and short-stroke stages was implemented. The first is an auxiliary stage (10) with sub-micrometer resolution and 10 mm gap range in a low-bandwidth closed-loop control. It is guided by an arrangement of six folded leafsprings, driven by a stepper motor and measured by an absolute encoder. The latter is the high-bandwidth module, consisting of the short-stroke frame, i.e. the metrology frame of the second crystals, and a reaction mass, the so-called balance mass (13). Both are equally guided by an arrangement of three folded leafsprings with respect to the long-stroke stage, providing the piston-tip-tilt DoFs for the second crystals with the ranges of ±2 mm and ±2 mrad. Then, following to a collocated design for optimized control options, the high-performance closed-loop control of the crystal cage is realized by means of three voice-coil force actuators between the short-stroke

frame and the balance mass, and an embedded interferometric system that directly measures the position between the metrology frames.

Finally, it is worth mentioning that, due to the cryogenic boundary conditions and beam interaction issues, the system must operate in ultra-high vacuum (UVH) of 10^{-9} mbar.

2.1 Performance specifications

Among the 3 high-bandwidth control loops of the crystal cage, i.e. gap, pitch and roll (also referred to as Y, Rx and Rz, according to the rotating coordinate system of the instrument around the x-axis, as shown in Figure 1), pitch is of particular attention. Indeed, it may affect not only the outgoing photon flux and energy bandwidth, but, with geometric lever-arms of tens of meters, also the position of the beam on the sample and the beam spot size due to vibration-related blurring effects. Because of that, the main target of this system is to hold the control error of the pitch DoF within 10 nrad_{RMS} (root mean square) in the frequency range between 1 Hz and 2.5 kHz, which contains nearly all of the relevant mechanical dynamics of the system at the same time that it covers typical detection time scales of beamline experiments. This target is put both for in-position operation mode, in which the experiments are performed with a fixed energy, and scanning operation mode, in which the energy varies over the experiment, requiring the main rotation and the gap to follow coordinated setpoints. For roll, there is a forgiveness factor of nearly 10 with respect to pitch requirements, thus, 90 nrad_{RMS} is defined as a target. For the gap, as much as 300 nm_{RMS} could be accepted. In practice, in meeting the requirements for pitch, the performances of roll and gap stay well below their specifications without additional effort.

2.2 System identification

The Frequency Response Function (FRF) of the short-stroke module (SHS) MIMO plant must be experimentally determined to better design the controller for the real application and to check if all the design effort to build a high-dynamic machine succeeded.

The first step is to impose a *white noise* broadband signal to the plant input in open loop. As the SHS has three inputs and three outputs, the identification is done by exciting each of the inputs sequentially and reading all outputs at the same time. Then, the FRFs are given simply by the division of the *power spectrum* of the output by the input signals. Although straightforward, this method has the disadvantage that the static position is not kept by a feedback controller during the identification. So, drifts may occur, and the identified signal may contain lower-frequency disturbances. Even though, having the first identified plant, the controller designer has an idea of the system resonances and of the magnitude of the plant FRFs. Then, with this information, one can derive a preliminary low-bandwidth controller to basically hold position for a subsequent identification. Indeed, at this point, the control loop can be closed, and the position error can be stabilized to a certain extent. This is desired because a sufficient Signal-to-Noise Ratio (SNR) is necessary to draw more reliable plant FRFs, which, in turn, requires the excitation signal power to be increased.

Next, a more well-defined excitation signal can be further used. One alternative is the multisine method, which consists of a simultaneous sum of sines in a finite number of frequencies, with specifically chosen phases and amplitudes. This excitation signal introduces a specific number of periods in the plant and excites the system just in those given frequencies, improving determinism and SNR. Another alternative is using just a sequence of sines with different frequencies and pre-determined amplitudes, the so-called single-sine method. This is the method used here to derive the MIMO identified plant depicted in Figure 2. Although more time consuming than the previously mentioned techniques, this decision was made to achieve a clearer identification of magnitude and phase of some peaks that proved to be critical in designing the controller.

Once the plant has been identified, additional analyses can be done. In particular, the Relative Gain Array (RGA) analysis, as defined in [4], indicates how well decoupled a MIMO system is over frequency. The closer the RGA is to the identity matrix (particularly around the control bandwidth frequency), the more decoupled the system is. Then, if sufficiently decoupled, the MIMO system can be addressed separately with SISO techniques, which considerably simplifies the controller design effort. Indeed, as it can be seen in Figure 2, by comparing the magnitudes in the rows and the columns of the matrix plot, the SHS is well decoupled up to about 1 kHz, such that, as long as the bandwidths of the SISO controllers stay below 1 kHz, the system shall not become unstable due to MIMO cross-talk interaction.

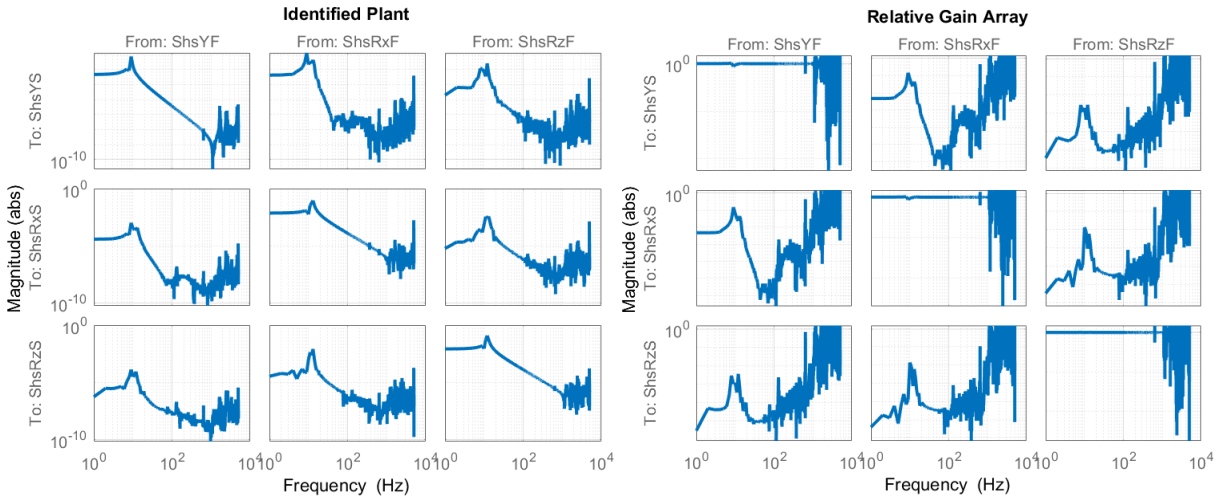

Figure 2 – Left: MIMO plant identification using single sine method. Right: Relative gain array plot for MIMO coupling analyses. The units are from force in N (Y) and torque in Nm (Rx and Rz) to displacement in meters (Y) and radians (Rx and Rz).

2.3 Controller design using loop-shaping method

The loop-shaping controller design method [3] consists in explicitly shaping the magnitude and the phase of the open-loop FRFs towards specific control targets. Here, as described in the previous section, the plant FRFs are the result of the system identification, such that actuators, sensors and data acquisition dynamics are already included. Then, the control engineer must add enough, but not more than necessary, control elements to the open-loop FRFs to achieve the desired closed-loop system performance, which here is defined as follows:

1. Phase Margin of 30°, for robustness;
2. Gain Margin of 8 dB, for robustness;
3. High low-frequency gain, for high trajectory following capacity;
4. Low high-frequency gain, for noise disturbance suppression.

All the controllers in the SHS have been designed as follows: a second-order low-pass filter with a corner frequency around 1000 Hz reduces the magnitude at high frequencies; one integrator with a cut-off frequency around 50 Hz increases the low frequency gain and trajectory following capacity; a lead filter increases the phase margin around the bandwidth frequency; notch filters reduce the magnitude of (otherwise bandwidth-limiting) poorly damped peaks; and, finally, the proportional gain meets the unit gain at the target bandwidth, in the range from 180 to 250 Hz for the 3 DoFs. In this application, all the high-frequency and high-magnitude peaks were extensively characterized, in order to confirm that their positions would not change during operation, which might compromise the system performance and stability.

This procedure consists of an iterative process in which the open-loop transfer functions are shaped and reshaped after calculating the required stability, robustness and performance indicators. Furthermore, considering that there are different operation modes with conflicting performance priorities, in addition to these standard controllers, multiple controllers may be designed, in which the designer may play with different bandwidths and/or low frequency gains.

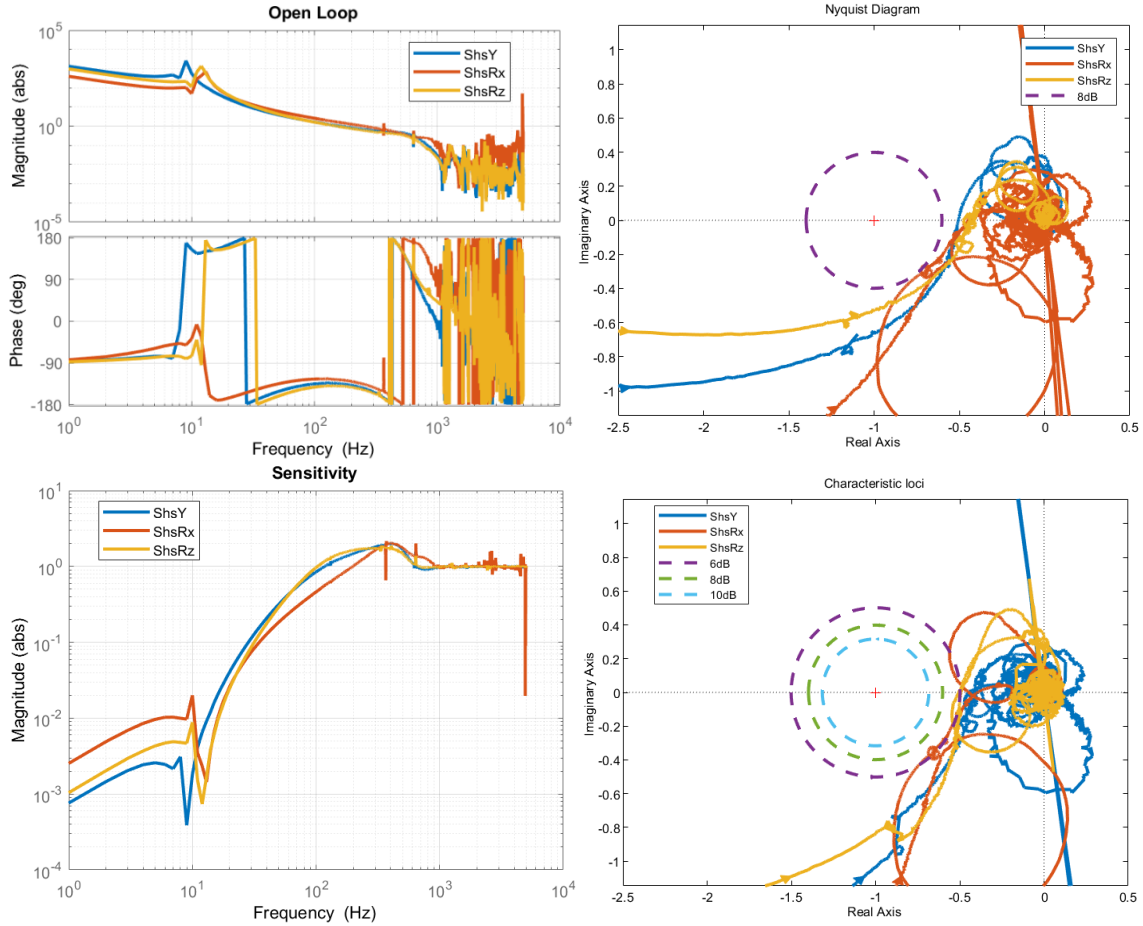

Figure 3 - Upper left: Open-loop plots of magnitude and phase of the 3-DoF SHS SISO system. Upper right: Sensitivity plot of the 3-DoF SHS SISO system. Bottom left: Nyquist plot of the 3-DoF SHS SISO system, with the robustness target circle of 8dB. Bottom right: Characteristic loci of the 3-DoF SHS system, analyzing the MIMO stability.

Figure 3 shows the results of the SISO controllers designed by the loop-shaping method for the SHS. In the open-loop Bode diagram, the higher gain in the low frequency range and suppressed amplitude for the high frequency range are clear from the magnitude plot, whereas the phase-margin can be seen at the bandwidth frequency in the phase plot. In the sensitivity plot, it can be seen that the curves do not exceed the magnitude of 2, which, simplistically put, is an equivalent design target for robustness and noise amplification purposes. Next, the Nyquist diagram attests not only for the stability of the individual controllers, but also for their robustness margins, in this case, better than 8 dB for all 3 loops. Finally, the *characteristic loci*, or *eigenvalue loci*, diagram, which is defined as the eigenvalues of the frequency response of the open-loop transfer function, provides a generalization of the Nyquist plot from SISO to MIMO systems [3]. Important to mention is that the circles depicted in the characteristic loci are not as valuable as in the SISO case (Nyquist diagram), because they do not represent the mathematical definition of stability, but they can be taken as a guideline in the MIMO analysis. Since the characteristic loci shown has a large resemblance with the SISO Nyquist diagram, it suggests that MIMO interaction hardly plays a role and the proposed SISO controller design approach is valid.

3. RESULTS

The following subsections present control performance results for the pitch (ShsRx) control loop, which is the most demanding and relevant DoF in the HD-DCM. These results were partly obtained with the machine in a test laboratory, but already under operational conditions, i.e. including cryogenics and vacuum, and partly obtained in its final environment at MANACÁ beamline in Sirius.

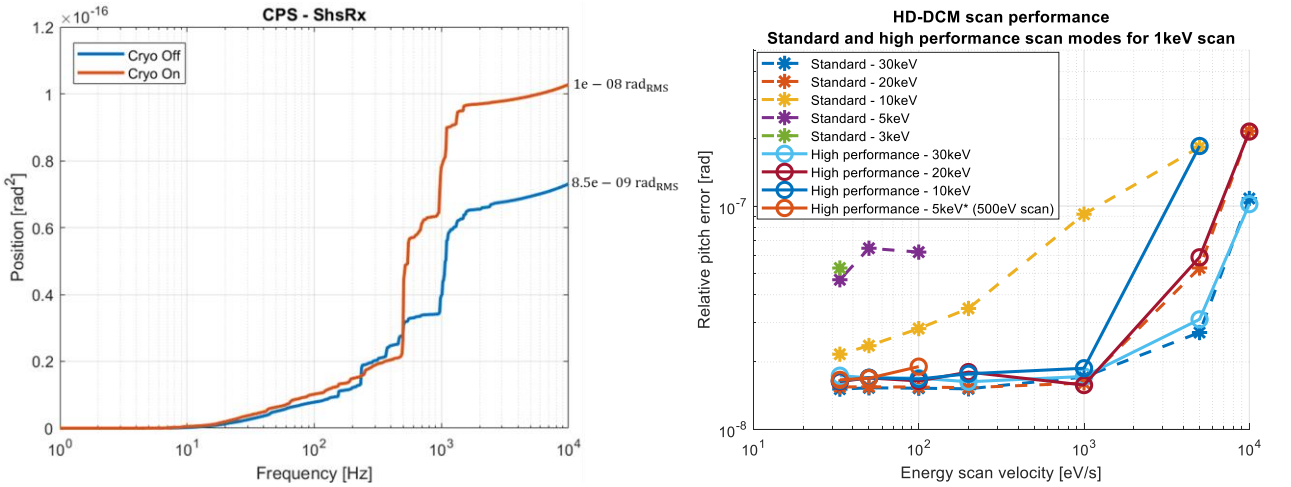

Figure 4 – Left: In-position control error cumulative power spectrum (CPS) for pitch (ShsRx), with and without recirculating cryogenic cooling. Right: Scanning RMS control error between 1 Hz and 2.5 kHz for pitch (ShsRx), in standard and high-performance modes, for a range of 1 keV and scanning velocities of 30 to 10.000 eV/s.

3.1 In-position performance

Analyzing the performance of the system as a function of frequency is essential not only to understand how the machine behaves to the different disturbance agents, but also to evaluate the impact of this spectral signature at the user's end. Therefore, the cumulative power spectrum (CPS) provides a convenient output format for performance analysis, with the partial integrated RMS value simply given by the square root of the data points.

The Figure 4 **Error! Reference source not found.** shows the in-position control error CPS for pitch (ShsRx) under the standard controller running at 20 kHz in NI CompactRIO platform (see [5]). Data sets of two different experimental conditions, namely, with and without liquid nitrogen flow, are shown for comparison. The error within the bandwidth is kept below 5 nrad_{RMS} and changes little between data sets, attesting that the additional flow disturbances are well suppressed in this range. At 1 kHz, a significant contribution is present in both sets. As detailed in [4], this corresponds to the second rocking mode of the metrology frame of the first crystals, which might be excited by electronic noise in the linear amplifier of the main rotary driver. Finally, the main difference between data sets lies in the contribution around 500 Hz, which, as also detailed in [4], corresponds to the first rocking mode of the metrology frame of the first crystals being excited by the flow-induced vibrations. As this is currently in the sensitivity peak of this control loop (see Figure 3), the disturbance effect is amplified, rather than suppressed. So, even though the system already meets its requirements, this is just the beginning for this machine and many aspects have already been mapped for improvements.

3.2 Trajectory following performance

Considering the dynamic concept of the HD-DCM, more interesting than the achieved in-position performance is the scanning capacity of the instrument, as compared to existing DCMs. The scanning performance is here evaluated considering the complete functional setpoint requirements, which include: the main rotary stage, driven by a direct drive with a closed-loop bandwidth of 20 Hz; the SHS system; and, optionally, the long-stroke stage. Indeed, thanks to the two-level design, two energy-scan modes are available, namely: standard and high-performance scanning.

In the standard mode, the Bragg angle is a setpoint to both the long-stroke and the short-stroke modules (explained in section 2 Mechanical design), which move together to adjust the nominal gap while the references for pitch and roll are generally fixed. Thus, scans of any range within the operational boundaries of the instrument can be made. However, the stepper-driven long-stroke actuator introduces significant mechanical disturbances in the system, lowering the control performance. Naturally, larger motion ranges and velocities, which are related to lower photon energies, i.e. energies between 3 and 10 keV, create more intense disturbances. In the high-performance scanning mode, on the other hand, the long-stroke is kept still while the Bragg setpoint is send to the SHS only. Then, although the scanning ranges become limited to feasible gap ranges within the short-stroke capabilities, the control errors can be equivalent to those of in-position performance. Unfortunately, 3 keV feasible scanning ranges are very limited and even at 5 keV scans in high-performance mode are limited to 500 eV only. Nonetheless, for scans at energies above 10 keV, the boundaries imposed by the high-performance mode bring no additional limitation.

These scanning results are also shown in Figure 4**Error! Reference source not found.**, with the control error RMS values for the ShsRx in scans in standard and high-performance modes. As cases of interest, 1 keV scans were made around different energy values for different speeds, so that every point in the graph corresponds to the total RMS value between 1 Hz and 2.5 kHz for a full scan at constant speed in eV/s. At speeds below 1 keV/s, it can be seen at the high-

energy end, i.e. above 20 keV, the angular and gap motions are so small that the performance is equivalent to that of in-position errors even in standard mode. At the opposite end, as the energy is reduced, however, the stroke and the speed of the long-stroke actuator increase, and the disturbing effects are clear, reaching as much as 80 $nrad_{RMS}$ at 3 keV. Above 1 keV/s, high speeds and accelerations are present, and the error levels increase. Nonetheless, significant improvement can be expected once feedforward control, which has not been implemented yet, is introduced. These scanning studies were carried out in the test lab with an xPC prototyping control platform running at 10 kHz (see [5]) in an earlier commissioning stage and shall be soon repeated at the beamline with the final hardware. Yet, it explains why the smallest numbers in the scanning plot do not meet the cryocooled performance displayed in the CPS plot.

To conclude, it is worth noticing that at 3 and 5 keV the scanning speeds were limited to 30 and 100 eV/s, respectively. This is due to a practical operational limit of about 1 mm/s in the variation of the gap between the crystals, which is partly given by the current speed limitations in the acquisition rate of the interferometers, but also related to acceleration levels and heat dissipation issues in the mechanics and actuators, respectively. For the future, this boundary is expected to be extended as well.

4. CONCLUSIONS

The complete controller design methodology for the high-bandwidth module of the HD-DCM for Sirius X-rays beamlines has been described. SISO feedback controllers were designed with loop-shaping after extensive MIMO plant identifications and RGA decoupling analyses, whereas stability and robustness have been attested according to well-established control plots and diagrams, such as sensitivity, Nyquist and characteristic loci. Finally, performance has been experimentally demonstrated in operational conditions. In particular, the control error performance of the pitch between crystals has proven to meet its specifications, not only in in-position fixed-energy operation mode, but also under demanding scanning conditions, with unprecedented dynamic performance becoming an enabling technology for science opportunities at the Brazilian Synchrotron Light Laboratory. Yet, as a newborn instrument there are still opportunities for optimization in design and control upgrades for performance improvement. In the near future, different controllers may be explored for specific operational conditions and feedforward control shall be implemented to reduce trajectory following errors.

5. ACKNOWLEDGEMENTS

The authors would like to gratefully acknowledge the funding by the Brazilian Ministry of Science, Technology, Innovation and Communication, and the contributions of the LNLS staff group and MI-Partners team.

6. REFERENCES

[1] Geraldes R R, et al. The Status of the New High-Dynamic DCM for Sirius. Proc. 10th Mechanical Engineering Design of Synchrotron Radiation Equipment and Instrumentation. 2018; 147-152.
[2] Rodrigues A R D, et al. Sirius Status Update. Proc. 10th International Particle Accelerator Conference. 2019; 1381-1384.
[3] Skogestad S, Postlethwaite I. Multivariable feedback control analysis and design. John Wiley and Sons, Inc. New York: 2001.
[4] Geraldes R R, et al. Dynamic Error Budgeting in the Development of the High-Dynamic Double-Crystal Monochromator for Sirius Light Source. ASPE Spring Topical Meeting, 2020.
[5] Moraes M A L, et al. The FPGA Control Implementation of the High-Dynamic Double-Crystal Monochromator at Sirius Light Source. ASPE Spring Topical Meeting, 2020.